UDC 54.057:547.83:547.792
DOI: 10.15587/2519-4852.2024.313808

DESIGN OF NON-COVALENT DUAL-ACTING INHIBITORS FOR PROTEASES M^{PRO} AND PL^{PRO} OF CORONAVIRUS SARS-COV-2 THROUGH EVOLUTIONARY LIBRARY GENERATION, PHARMACOPHORE PROFILE MATCHING, AND MOLECULAR DOCKING CALCULATIONS

Larysa Yevsieieva, Pavlo Trostianko, Alexander Kyrychenko, Volodymyr Ivanov, Sergiy M. Kovalenko, Oleg Kalugin

The proteases of the SARS-CoV-2 coronavirus are crucial for the virus's life cycle, making them a prime target for developing antiviral drugs to combat COVID-19. Currently, there is a priority to develop new antiviral drugs that can target multiple viral proteins at once. In this study, we analyze the molecular mechanisms of how non-covalent inhibitors interact with the main protease (M^{pro}) and papain-like (PL^{pro}) protease of SARS-CoV-2 to create a computer modelling algorithm for discovering ligands that can inhibit both M^{pro} and PL^{pro} simultaneously.

Aim of the study. *We aim to analyze the molecular structures involved in the interactions between current non-covalent inhibitors and the M^{pro} and PL^{pro} proteases of SARS-CoV-2. The goal is to identify a common molecular structure that could be used to discover new inhibitors with a dual-acting mode using computer simulations.*

Materials and methods. *LigandScout 4.5 software was used for 3D-pharmacophore analysis, virtual screening and molecular docking. AutoDock Vina 1.1.2 tools was utilized for molecular docking. Web-servers PLIP (Protein-Ligand Interaction Profiler) and Pharmit were used for studying molecular binding mechanisms. Generation of evolutionary libraries was performed by DataWarrior 6.0. Analysis and visualization were performed by Discovery Studio 2024 Suite.*

Results. *Our study analyzed various models of SARS-CoV-2 protease binding sites available in the Protein Data Bank (PDB) and their corresponding non-covalent inhibitor ligands. This analysis helped identify important features of the M^{pro} and PL^{pro} ligands. By comparing the pharmacophore models of M^{pro} ligands with the structural features of PL^{pro} inhibitors, we identified ligands that could potentially match the binding sites of both proteases. Using the structures of these ligands, an evolutionary library was created in the DataWarrior program. Virtual screening of this library using both M^{pro} and PL^{pro} pharmacophores revealed several new hit molecules. Molecular docking of these molecules into the active sites of the M^{pro} and PL^{pro} proteases and calculating their binding energetics led to the identification of several molecules and their corresponding scaffolds with dual inhibition potential. These findings can be further studied in vitro with the aim of discovering drugs for COVID-19.*

Conclusions. *We used computer-based screening to search for ligands that could bind to both M^{pro} and PL^{pro} proteases. After identifying these potential compounds, we developed synthesis methods to obtain them for further in vitro biological activity studies*

Keywords*: SARS-CoV-2, M^{pro} protease, PL^{pro} protease, dual inhibitors, virtual pharmacophore screening, docking*

How to cite:
Yevsieieva, L., Trostianko, P., Kyrychenko, A., Ivanov, V., Kovalenko, S. M., Kalugin, O. (2024). Design of non-covalent dual-acting inhibitors for proteases M^{PRO} and PL^{PRO} of coronavirus SARS-CoV-2 through evolutionary library generation, pharmacophore profile matching, and molecular docking calculations. ScienceRise: Pharmaceutical Science, 6 (52), 15–26. http://doi.org/10.15587/2519-4852.2024.313808

1. Introduction

The main protease (M^{pro}) and papain-like protease (PL^{pro}) are crucial enzymes in the replication of the SARS-CoV-2 coronavirus, and they are potential targets for drug development against SARS-CoV-2 [1]. Inhibiting Mpro has shown promise as a method for developing therapeutics for COVID-19 [2]. M^{pro} plays a role in cleaving viral polyproteins into functional proteins necessary for viral replication and assembly in the host cell. Inhibitors of M^{pro} can block this process. Targeting the main protease of SARS-CoV-2 is advantageous due to the conservation of M^{pro}. Despite mutations observed in the coronavirus family, M^{pro} exhibits high sequence and structural similarity among different strains [3]. This suggests that M^{pro} inhibitors may be effective against various strains and types of coronaviruses.

Papain-like protease (PL^{pro}) has also become an important biological target for the development of antiviral drugs since it is also involved in the formation of functional viral proteins necessary for its successful replication in cells [4].

The combination of several mechanisms of influence on a viral infection or its consequences is now an urgent task for the development of new drugs against COVID-19. Dual inhibitors can simultaneously target multiple pathways involved in viral replication. This comprehensive approach to combating SARS-CoV-2 may reduce the likelihood of resistance to drugs target-

ing a single enzyme and increase the effectiveness of antiviral treatments [5].

Understanding the mechanisms of inhibition helps to find opportunities to model molecules that act on the active sites of M^{pro} and PL^{pro} proteases simultaneously [6]. Studying the 3D structures of M^{pro} and PL^{pro} with various inhibitors shows the specificity and features of the interaction of the protein with the inhibitor ligand, which is accordingly reflected in the kinetic binding profiles and structural features of the ligand molecules. Protease inhibitors are classified based on their binding kinetics as covalent and non-covalent inhibitors [3].

Covalent inhibitors can provide stronger and longer-lasting inhibition, making them effective in some scenarios. However, they also pose an increased risk of side effects due to the stable covalent bonds, which can potentially increase toxicity. M^{pro} has a catalytic binary Cys-His structure, unlike other chymotrypsin-like and many serine or cysteine proteases, and no known human proteases share their cleavage sites [7]. In the case of M^{pro}, using covalent inhibitors might be a logical approach because of M^{pro}'s specificity. Covalent M^{pro} inhibitors are known for targeting Cys145 precisely. Reversible covalent inhibitors create a bond with the cysteine at the active site of M^{pro} that can be reversed. Examples of reversible covalent M^{pro} inhibitors are Boceprevir and Nirmatrelvir. On the other hand, irreversible covalent inhibitors can block M^{pro} by forming an irreversible covalent bond with the catalytic cysteine residue [3].

There is a growing interest in non-covalent M^{pro} inhibitors. Ensitrelvir (S-217622) is a new non-covalent M^{pro} inhibitor discovered through virtual screening, and it has been approved by the FDA [8]. In March 2024, Shionogi & Co., Ltd. (Japan) announced that Xocova® (ensitrelvir fumaric acid) has received standard approval for the treatment of SARS-CoV-2 infection. Xocova® is the first antiviral drug for COVID-19 treatment to receive standard approval in Japan, based on positive results from the Phase 3 portion of the Phase 2/3 study (SCORPIO-SR) [9].

Non-covalent inhibitors competitively bind to the catalytic site via specific hydrogen bonds and nonpolar interactions, ultimately blocking access to the catalytic site and preventing the protease from performing its biological function [10, 11].

Non-covalent inhibitors are preferable because they are less likely to cause non-specific interactions and potentially reduce side effects. They are commonly used for PL^{pro} because they can interact reversibly with the enzyme's active site without forming stable covalent bonds. This approach may be a rational solution for PL^{pro} because the N-terminal ubiquitin-like (Ubl) domain of PL^{pro} is not specific and shares similarities with human cellular DUBs. Developing covalent viral protease-specific PL^{pro} inhibitors without blocking cellular human deubiquitinating (DUB) enzymes may be difficult and require extensive safety studies [12].

The search for more effective drugs for the treatment of COVID-19 involves developing new dual non-covalent inhibitors to simultaneously target the key proteases M^{pro} and PL^{pro} of the SARS-CoV-2 virus [1].

The recent study has reported compounds identified as dual-acting SARS-CoV-2 protease inhibitors that target both M^{pro} and PL^{pro} (Mpro IC_{50}=1.72±0.75 μM, PL^{pro} IC_{50}=0.67±0.59 μM) [13] (Fig. 1, *a*, *b*).

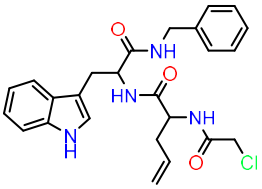

M^{pro} IC_{50}=5.01±2.31

PL^{pro} IC_{50}>25

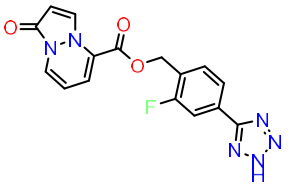

M^{pro} $\Delta G_{binding}$=-7.8 kcal/mol

PL^{pro} $\Delta G_{binding}$=-9.1 kcal/mol

Fig. 1. Dual-targeting inhibitors against SARS-CoV-2 proteases: *a* – primary targeting M^{pro} according to cellular screening; *b* – primary targeting PL^{pro} according to molecular docking studies [13, 14]

Several compounds with the general structural formula, shown in Fig. 1, have been suggested in experimental and computational studies as non-covalent dual inhibitors of M^{pro} and PL^{pro} [14].

Using computer modelling of a double covalent inhibitor, the authors determined that the electrophilic imine carbon and the chlorinated carbon of the quinoline fragment are accessible to nucleophilic attack by the sulfur atom of the active centre of the cysteine proteases M^{pro} and PL^{pro} [15]. As a result of the studies, three molecules showed inhibitory activity against two proteases (Fig. 2).

Potential antiviral compounds have been discovered using the E-pharmacophore hypothesis, created from a complex of two models: the non-covalent ligand GRL0617-PL^{pro} and the non-covalent ligand X77-M^{pro} [5]. After the screening phase of the proposed pharmacophore hypothesis and docking into the corresponding ligand-protease models, cytonic acid A and cytonic acid B were proposed as compounds having significant interactions with both PL^{pro} and M^{pro} proteases (Fig. 3).

Ligand 1

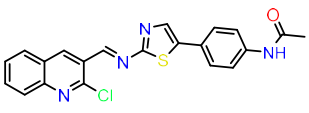

M^{pro} *Ki* (μM)=1.63±0.30

PL^{pro} *Ki* (μM)=1.20±0.15

Ligand 2

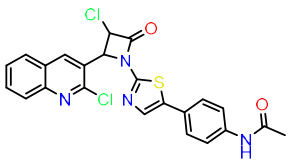

M^{pro} Ki (μM)=0.82±0.12

PL^{pro} Ki (μM)=0.35±0.10

Ligand 3

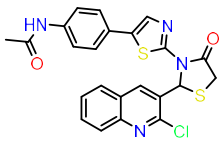

M^{pro} Ki (μM)=6.07±0.53

PL^{pro} Ki (μM)=8.75±0.87

Fig. 2. Dual-targeting inhibitors against M^{pro} and PL^{pro} enzymes [15]

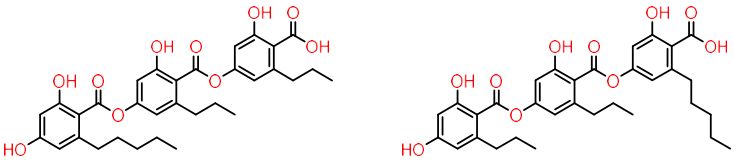

Cytonic acid A
PubChem CID 491708

Cytonic acid B
PubChem CID 491709

Fig. 3. Structure of cytonic acid A and cytonic acid B, proposed as dual inhibitors of M^{pro} and PL^{pro} enzymes [15]

2. Planning (methodology) of the study

Since the active center shape of each protease is specific and the interaction of different ligands with the active center of the protease has its own specificity, we used a procedure for initial filtering using 3D pharmacophores of various PDB ligand-protease structures [16, 17]. This process was carried out to identify common parameters suitable for binding with both M^{pro} and PL^{pro} (Fig. 4).

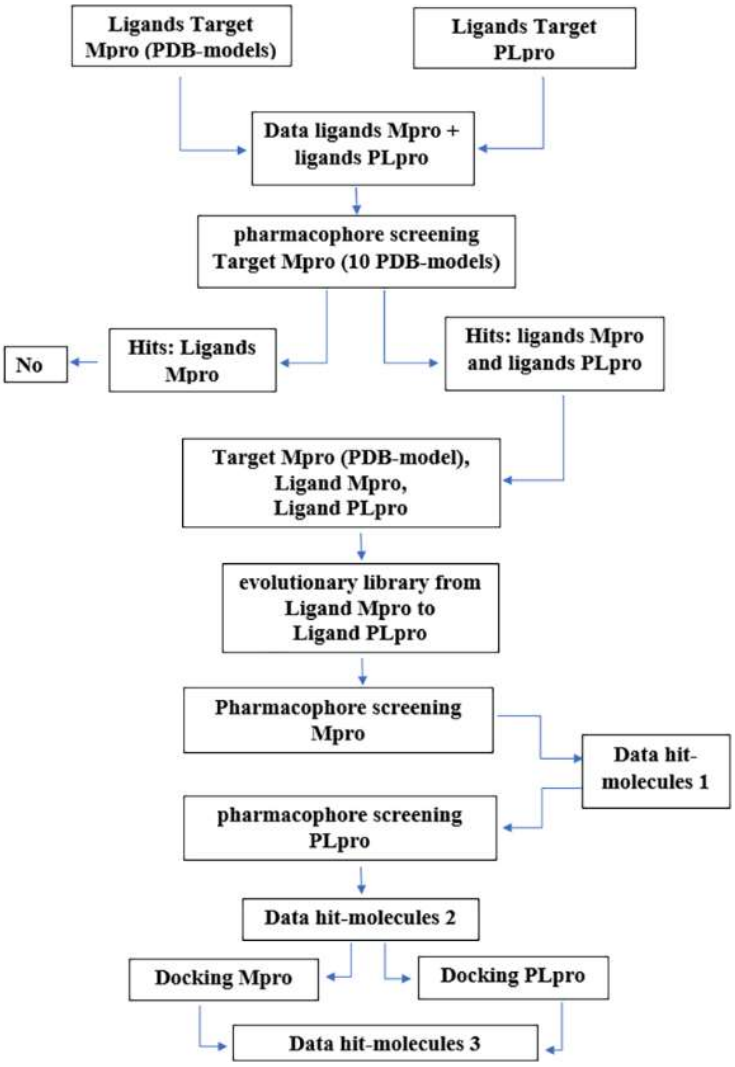

Fig. 4. Algorithm for discovering non-covalent dual-action inhibitors against SARS-CoV-2 protease M^{pro} and PL^{pro}

When searching for biologically active molecules with specific properties, a combination of virtual screening (VS) and molecular docking is usually used. In virtual screening, pharmacophore models are developed using crystal structures of protease active sites and various inhibitors from the PDB database. The potential hits identified through virtual screening are then validated through a molecular docking process and assessed for pharmacokinetic parameters [18].

Therefore, in this study, we suggested and applied a new original algorithm for developing some potent non-covalent dual-acting inhibitors of M^{pro} and PL^{pro} using a number of X-ray PDB structures of the complexes of SARS-CoV-2 M^{pro} and PL^{pro} with non-covalent inhibitors (Fig. 4).

Briefly, the algorithm starts the pharmacophore screening of the Evolutionary library against the M^{pro} pharmacophore, leading to Data hit-molecules 1. The pharmacophore screening of this database against the PL^{pro} pharmacophore selected Data hit-molecules 2. The last database – Data hit-molecule 3, is formed based on the docking results of the hit-molecule database 2. The selected ligands, which have binding affinity values for both proteases of at least 90 % from the corresponding value for the reference ligand of the ligand-protease complex M^{pro} and PL^{pro}. At this step, further library optimization was performed against the Murcko scaffold, as described in detail in Fig. 9, 10.

3. Materials and Methods

Molecular ligand analysis and design of new bioactive molecules were performed using LigandScout 4.5 [19], which allowed for pharmacophore analysis and virtual screening of defined molecular databases against the generated pharmacophores. LigandScout tools were used to define the parameters of molecules that would correspond to drug-like properties. Molecules with poor permeability and oral absorption (molecular weight>500, C log*P*>5, more than five hydrogen bond donors and more than ten acceptor groups) were excluded [20].

DataWarrior software [21] was used to create the evolutionary library, calculate the physicochemical properties and analyze the molecular scaffolds. X-ray crystal structures of the target proteins were obtained from the Protein Data Bank [22] and used for virtual screening and receptor-based docking. Receptor-based docking was performed using the AutoDock Vina program [23, 24].

PLIP (Protein-Ligand Interaction Profiler) [25] and Pharmit web server [26] for studying molecular binding mechanisms. Analysis and visualization were performed using Discovery Studio 2024 Suite.

The reagents used in this work were manufactured by Sigma-Aldrich (USA) and were purified using standard techniques. Control of the reactions was monitored using thin-layer chromatography on “Sorbfil UV-254” plates with an eluent of ethyl

acetate-hexane (1:2 ratio). ^{1}H NMR spectra were recorded on Varian Gemini 400 MHz spectrometers using dimethyl sulfoxide (DMSO-d6) as the solvent. LC/MS spectra were recorded using a PE SCIEX API 150EX liquid chromatograph equipped with a UV detector (λ_{max} 215 and 254 nm) and a Luna-C18 column, Phenomenex (100×4 mm). Elution started with water and ended with acetonitrile/water (95:5, v/v) using a linear gradient at a flow rate of 0.15 mL/min and an analysis cycle time of 25 min.

4. Research result

4. 1. Structure-based virtual screening

To study the mechanisms of inhibition of the M^{pro} and PL^{pro} proteases of the SARS-CoV-2 virus, we selected a number of different models of binding sites for each protease with various non-covalent inhibitor ligands available from the Protein Data Bank (PDB).

Fig. 5 shows the main non-covalent M^{pro} inhibitors and M^{pro} binding sites presented in the PDB three-dimensional structures of biological macromolecules.

Fig. 6 shows the main non-covalent PL^{pro} inhibitors and PL^{pro} binding sites presented in the PDB three-dimensional structures of biological macromolecules.

We studied the molecular mechanisms of binding of the non-covalent SARS-CoV-2 protease inhibitors M^{pro} and PL^{pro} to their targets using the PLIP (Protein-Ligand Interaction Profiler) application [27] and the Pharmit resource: interactive exploration of chemical space [28].

To build a new large chemical space of ligands active against M^{pro}, we first generated an Evolutionary library starting from representative Ligand 7XB (Fig. 5, PDB: 7EN8) using DataWarrior software [21]. The evolutionary algorithm mimicked the natural evolution of drug-like compounds. The algorithm starts with a parent Ligand 7XB called the first generation. Next, a series of similar derivatives were built by applying a minor random structural modification of a parent structure. Each new structural modification is then evaluated based on how much it fits within customizable fitness criteria, such as molecular weight (Mw), cLogP, polar surface area (PSA), and so on [17]. The generated evolutionary library contained about 70000 ligands.

Studying the molecular mechanisms of substrate-ligand binding made it possible to find pharmacophoric features for non-covalent ligand inhibitors of each SARS-CoV-2 protease [29].

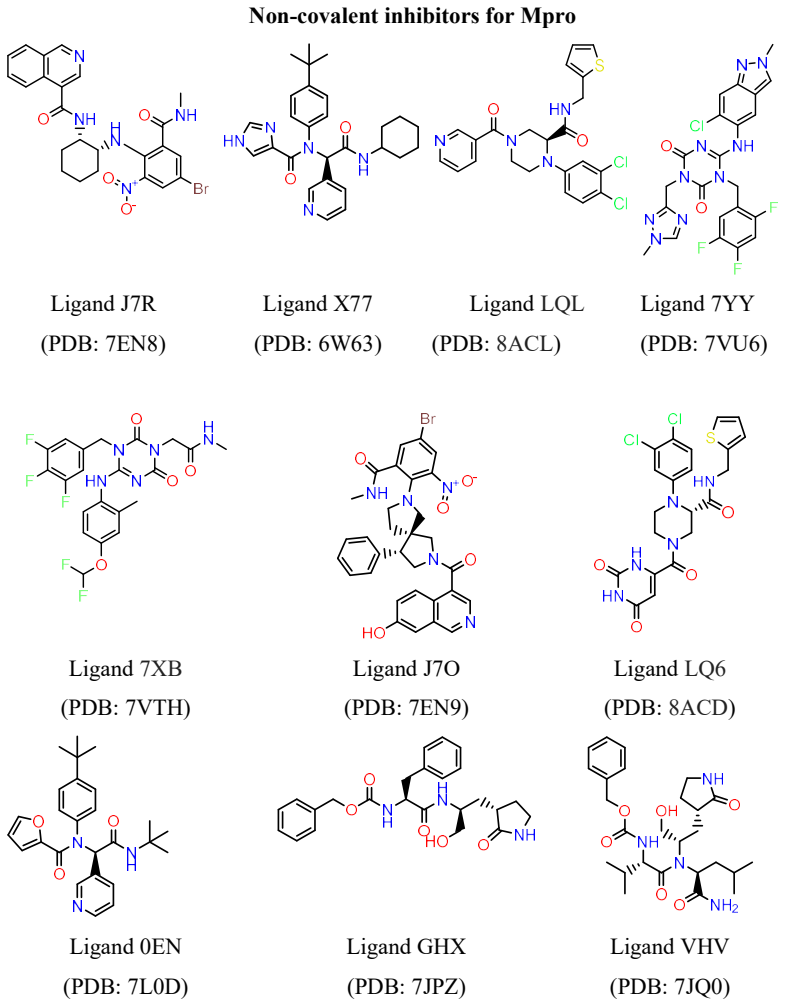

Fig. 5. Structures of non-covalent M^{pro} inhibitors. The corresponding PDB codes are given in brackets

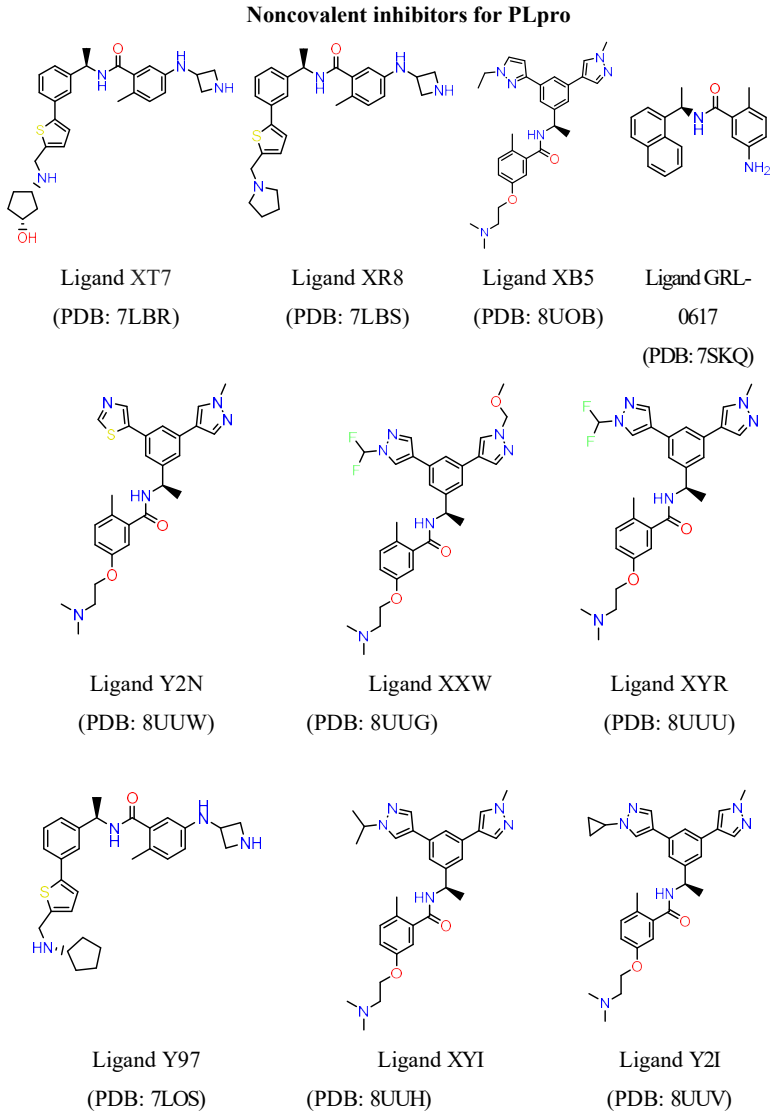

Fig. 6. Structures of noncovalent inhibitor of PL^{pro}. The corresponding PDB codes are given in brackets

The noncovalent M^{pro} inhibitors bind to the receptor through: a) hydrophobic fragments located in the area of residues 25 THR: 26 THR and/or 41 HIS, as well as in the region of residues 163HIS and 189GLN; b) interactions that create a hydrogen bond with the protease side chain donor in the region of residues 165MET:166 GLU and 143GLY:145 SER (as shown in Fig. 7A) [19, 25].

Analysis of the molecular features of the PL^{pro}-ligand interaction showed the predominance of hydrophobic interactions: residues for non-covalent binding include Tyr268, Gln269, Arg167, which are involved in van der Waals interactions. Interactions that form a hydrogen bond with the protease side chain donor are located in the region of residues 268TYR, 269GLN and 273TYR (Fig. 7 B) [19, 25].

In silico screening was conducted to identify noncovalent inhibitors for two SARS-CoV-2 proteases, M^{pro} and PL^{pro}. The 3D pharmacophores of 10 M^{pro} binding sites were used to determine the structures of M^{pro} active site. The pharmacophore models identified PL^{pro} ligands as hits (Table 1), which enabled the study of the potential for a dual mechanism of inhibition.

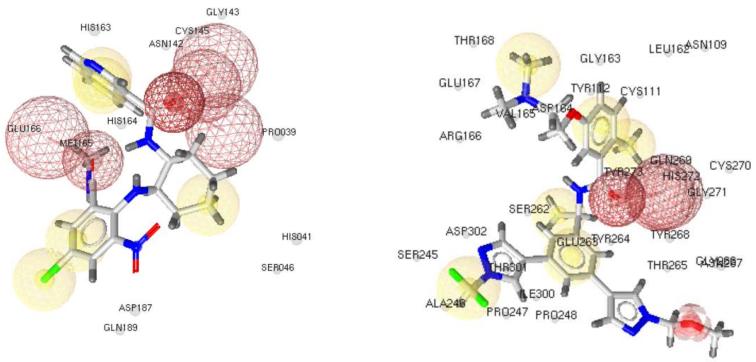

Fig. 7. 3D-pharmacophores A) Ligand J7R (M^{pro} PDB: 7EN8) and B) Ligand XXW (PL^{pro} PDB: 8UUG), LigandScout 4.5 program [19]

Table 1

Results of screening of non-covalent PL^{pro} inhibitors against pharmacophores of M^{pro} models, where 0 – no result, 1 – a match between the PL^{pro} ligand and the M^{pro} pharmacophore was found.

M^{pro} / PL^{pro}		Ligand J7R	Ligand X77	Ligand LQL	Ligand 7YY	Ligand 7XB	Ligand J7O	Ligand LQ6	Ligand 0EN	Ligand GHX	Ligand VHV
Ligand PDB		PDB: 7EN8	PDB: 6W63	PDB: 8ACL	PDB: 7VU6	PDB: 7VTH	PDB: 7EN9	PDB: 8ACD	PDB: 7L0D	PDB: 7JPZ	PDB: 7JQ0
XT7	7LBR	0	0	0	0	0	0	0	0	0	0
XR8	7LBS	0	0	0	0	0	0	0	0	0	0
XB5	8UOB	0	0	0	0	0	1	0	0	0	0
GRL-0617	7SKQ	0	0	0	0	0	0	0	0	0	0
Y2N	8UUW	0	0	1	0	0	0	0	0	0	0
XXW	8UUG	1	1	0	0	0	0	0	0	0	0
XYR	8UUU	1	0	0	0	0	0	0	0	0	0
Y97	7LOS	0	0	0	0	0	0	0	0	0	0
XYI	8UUH	0	0	0	0	0	0	0	0	0	0
Y2I	8UUV	0	0	0	0	0	0	0	0	0	0

The presence of certain common pharmacophoric features in some ligands, PL^{pro} (ligand XXW PDB: 8UUG) and M^{pro} (ligand J7R PDB: 7EN8) suggests the existence of a set of molecules with similar structures to both ligands and the potential to inhibit two proteases, M^{pro} and PL^{pro}. To test this hypothesis and identify the corresponding molecules, we generated a diverse library of compounds using the DataWarrior program [21] based on ligand J7R from the active site of M^{pro} (PDB: 7EN8) and ligand XXW from the active site of PL^{pro} (PDB: 8UUG).

Further filtering of compounds using VS screening against the corresponding pharmacophore model M^{pro} PDB:7EN8 and then PL^{pro} PDB:8UUG identified molecules with a likely dual mechanism of inhibition for M^{pro} and PL^{pro}.

4. 2. Docking Modeling and Identification of Molecules with Dual-Acting Inhibition Potential for M^{pro} and PL^{pro}

Molecular docking into the binding pockets of M^{pro} and PL^{pro} and determination of the energetic characteristics of ligand-protease complexes made it possible to identify a number of structures with good energetic characteristics for the binding to both proteases.

DataWarrior software visually presents the relationship between the energy values of ligands and their ability to bind to target proteins. Specifically, it shows the correlation between AutoDock Vina Binding Affinity (kcal/mol) and LigandScout Binding Affinity Score (BAS) (Fig. 8). Lower values on the graph indicate more stable complexes. Ligands with the lowest scores are typically considered promising for further research. To identify active molecules, we considered their binding affinity value (kcal/mol) to be at least 90 % of or exceeding the corresponding affinity value for the reference ligand of the ligand-protease complex. The same method was applied when analyzing the BAS values. The molecular docking results for ligands from the evolutionary library into the binding pockets of M^{pro} PDB:7EN8 and PL^{pro} PDB:8UUG are summarized in Fig. 8.

Using the DataWarrior tool, we filtered and grouped molecules by their Murcko scaffold. This helped to focus on the main structure of molecules without side chains, which determines the molecule's activity (Fig. 9, 10) [21].

The calculated binding energies for several of the examined ligands in the molecule-protease complex were comparable to those of native ligands. This indicates that these molecules may have the potential to inhibit both the M^{pro} and PL^{pro} proteases. These molecules share a common Murcko scaffold (Fig. 11), which suggests that they could be chosen for further studies.

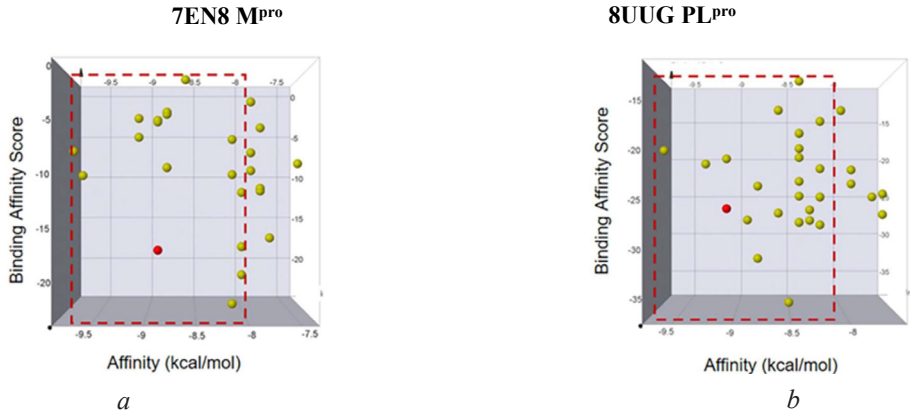

a *b*

Fig. 8. Graphical representation of the docking results. A ligand distribution according to the binding affinity in ligand-protease complexes: *a* – M^{pro} from 7EN8; *b* – M^{pro} from 8UUG. The corresponding PDP ligand molecule taken from the protease active center model is marked *in red*

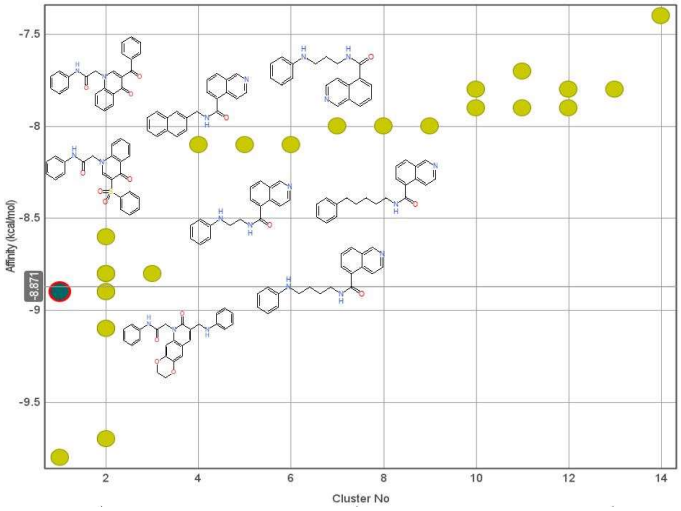

Fig. 9. Graphical representation of the results of docking of M^{pro} molecule-protease complexes (PDB:7EN8): distribution of Murcko scaffold clusters of molecules by Affinity value (the ligand molecule PDB:7EN8 is marked *in blue*)

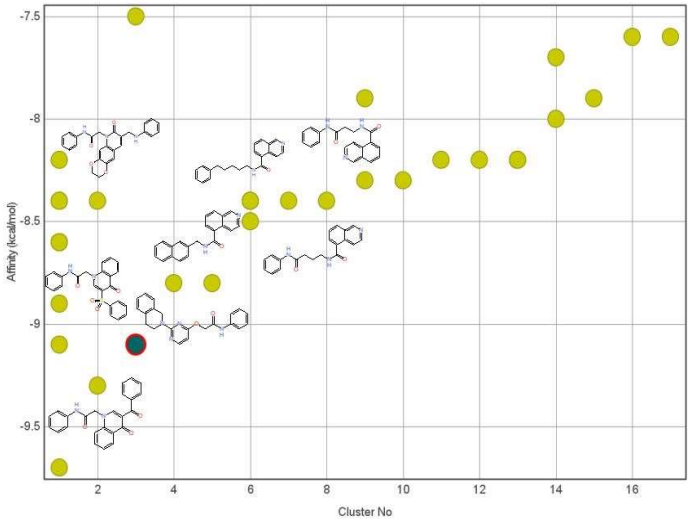

Fig. 10. Graphical representation of the results of docking of molecule-protease complexes PL^{pro} (PDB: 8UUG): distribution of Murcko scaffold clusters of molecules by Affinity value (ligand molecule PDB: 8UUG is marked *in blue*)

4. 3. Chemistry

For the selected hits, we developed and implemented retrosynthetic procedures in accordance with our previously published methods [25–27] (Fig. 12). The structure and purity of the obtained substances were proven by ^{1}H-NMR and LC/MS spectral methods.

The synthesis scheme for 2-(6-ethyl-4-oxoquinolin-1(4H)-yl)-N-phenylacetamide derivatives (**6, 10a-c**) is shown in Fig. 12. Key intermediates (**4, 9a-b**) were obtained by the Gold-Jacobs reaction of ethyl 2-benzoyl-3-(dimethylamino)acrylate (**3**) or ethyl 3-(dimethylamino)-2-(arylsulfonyl)acrylates (**8a-b**) using a reported procedure [30].

Then, these core building blocks (**4, 9a-b**) were alkylated with substituted chloroacetamides (**5a-d**) in DMF in the presence of sodium hydride [31] and provided targeted products (**6, 10a-c**).

The key intermediate (**15**) of the synthesis of *N*-(2-fluorophenyl)-2-(7-oxo-8-((phenylamino) methyl)-2,3-dihydro-[1,4]dioxino[2,3-g]quinolin-6(7*H*)-yl)acetamide (**16**) was obtained by a previously developed method, as summarized in Fig. 13 [28]. Alkylation was performed using an analogous procedure as for the derivatives of ethylquinolin-4(1H)-one (**4**, **9a-b**) using 2-chloro-N-(2-fluorophenyl)acetamide (**5e**) [31].

*General Procedure for alkylation of substituted 6-ethylquinolin-4(1H)-ones (**4, 9a-b**).*

Sodium hydride, 60% dispersion in mineral oil (200 mg, 5 mmol) was washed on a glass filter with anhydrous THF, then added to a solution of the corresponding 6ethylquinolin-4(1H)-one (**4, 9a-b**) (1 mmol) in anhydrous DMF (10 mL) and the mixture was stirred at rt for 30 min. Then, the reaction mixture was heated to 40ºC, and the corresponding chloroacetamide (**5a-d**) (1.2 mmol) was slowly added. The resulting mixture was stirred for 4 h at 70 °C, cooled to rt and diluted with water (40 mL). The formed precipitate was filtered off, washed with water and recrystallized from i-PrOH to get pure products (**6, 10a-c)** in 78–90 % yield.

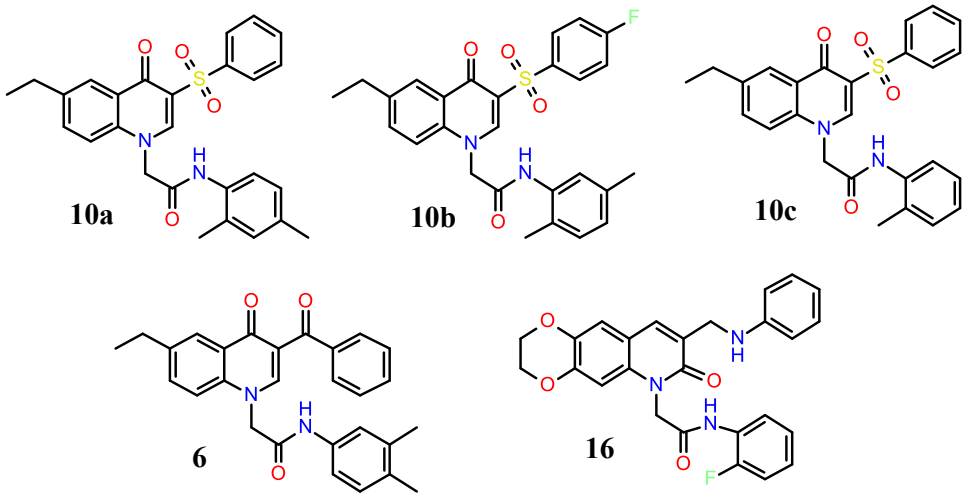

Fig. 11. Some ligands (**6, 10a-c, 16**) with common Murcko scaffolds (**SF1 – SF3**)

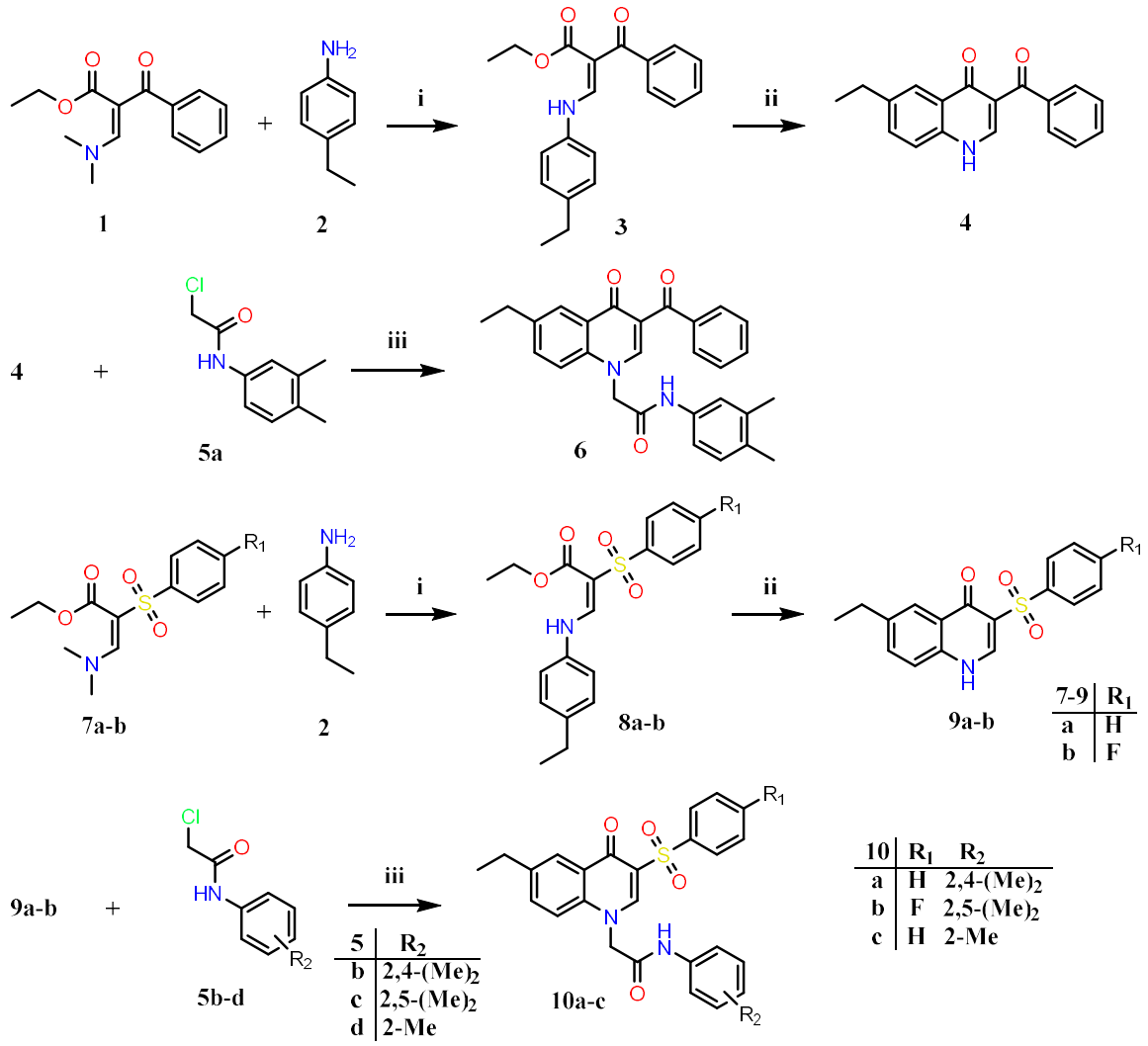

Fig. 12. Scheme for the synthesis of 2-(6-ethyl-4-oxoquinolin-1(4*H*)-yl)-*N*-phenylacetamide derivatives (**6, 10a-c**). *i*: iPrOH, reflux, 2h; *ii*: $(Ph)_2O$, reflux, 30 min; *iii*: DMF, NaH, 70°C, 4 h.

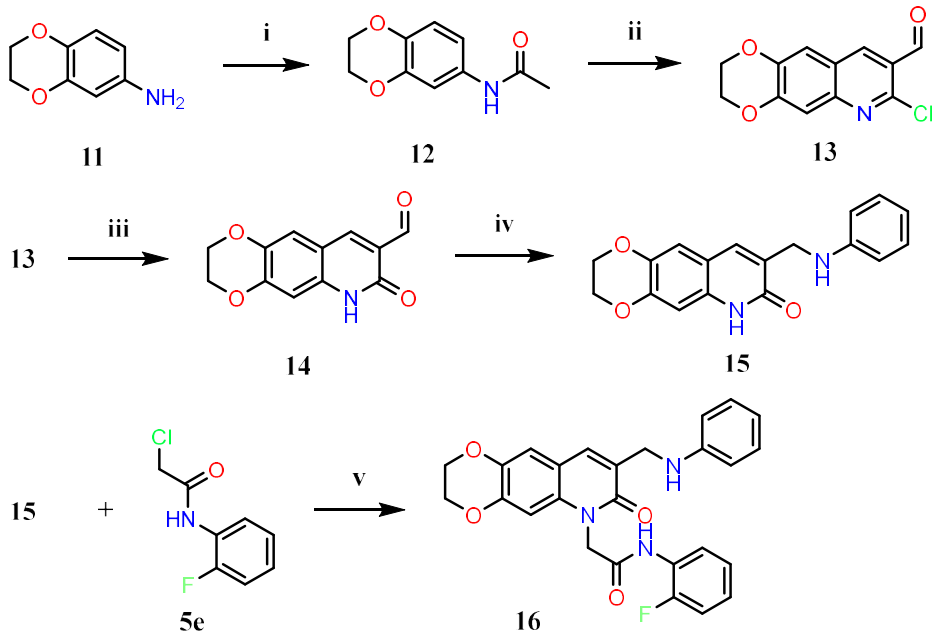

Fig. 13. Scheme for the synthesis of *N*-(2-fluorophenyl)-2-(7-oxo-8-((phenylamino)methyl)-2,3-dihydro-[1,4] dioxino[2,3-g]quinolin-6-(7*H*)-yl)acetamide (**16**). i: Ac_2O, rt, 30 min; ii: DMF, $POCl_3$, rt, 1h; iii: CH_3COOH, H_2O, reflux, 4 h; iv: THF, $PhNH_2$, $NaBH_3CN$, 70°C, 1 h; v: DMF, NaH, 70 °C, 4 h.

*2-(3-Benzoyl-6-ethyl-4-oxoquinolin-1(4H)-yl)-N-(3,4-dimethylphenyl)acetamide (**6**).*

White crystals, mp>300 °C. ^{1}H NMR: (400 MHz, DMSO-d6) δ 10.2 (*s*, 1H), 8.24 (*s*, 1H), 8.02 (*d*, *J*=2.5 Hz, 1H), 7.72 (*m*, 2H), 7.65–7.33 (*m*, 6H), 7.27 (*d*, *J*=10 Hz, 1H), 7.06 (*d*, *J*=9.6 Hz, 1H), 5.12 (*s*, 2H), 2.72 (*q*, *J*=8 Hz, 2H), 2.16 (*s*, 6H), 1.20 (*t*, *J*=5.2 Hz, 3H). $[MH]^+$ m/z=439.3.

*N-(2,4-Dimethylphenyl)-2-(6-ethyl-4-oxo-3-(phenylsulfonyl)quinolin-1(4H)-yl)-acetamide (**10a**).*

White powder, mp>300 °C. ^{1}H NMR: (400 MHz, DMSO-d6) δ 9.88 (s, 1H), 8.91 (s, 1H), 7.99 (t, J=5 Hz, 3H), 7.80 – 7.45 (m, 5H), 7.22 (d, J=10 Hz, 1H), 7.01 (s, 1H), 6.93 (d, J=8 Hz, 1H), 5.40 (s, 2H), 2.70 (q, J=6 Hz, 2H), 2.20 (d, J=4 Hz, 6H) 1.16 (t, J=5 Hz, 3H). $[MH]^+$ m/z=475.2.

*N-(2,5-Dimethylphenyl)-2-(6-ethyl-3-((4-fluorophenyl)sulfonyl)-4-oxoquinolin-(4H)-yl)acetamide (**10b**).*

White powder, mp>300 °C. ^{1}H NMR: (400 MHz, DMSO-d6) δ 9.86 (*s*, 1H), 8.91 (*s*, 1H), 8.09 (*q*, *J*=2 Hz, 2H), 7.93 (*s*, 1H), 7.74 (*d*, *J*=10vHz, 1H), 7.58 (*d*, *J*=8 Hz, 1H), 7.42 (*t*, *J*=8 Hz, 2H), 7.22 (*s*, 1H), 7.08 (*d*, *J*=7 Hz, 1H), 6.89 (*d*, *J*=7 Hz, 1H), 5.42 (*s*, 2H), 2.69 (*q*, *J*=6 Hz, 2H), 2.19 (*s*, 6H), 1.15 (*t*, *J*=6 Hz, 3H). $[MH]^+$ m/z=493.2.

*2-(6-Ethyl-4-oxo-3-(phenylsulfonyl)quinolin-1(4H)-yl)-N-(o-tolyl)acetamide (**10c**).*

White crystals, mp>300 °C. ^{1}H NMR: (400 MHz, DMSO-d6) δ 10.55 – 9.20 (*s*, 1H), 8.96 (*s*, 1H), 8.14 (*d*, *J*=8 Hz, 1H), 8.01 (*d*, *J*=4 Hz, 2H), 7.82 (*t*, *J*=4 Hz, 1H), 7.72–7.42 (m, 4H), 7.39 (*d*, J=4 Hz, 1H), 7.30–7.00 (*m*, 3H), 5.45 (*s*, 2H), 2.71 (*q*, *J*=6.5 Hz, 2H), 2.20 (*s*, 3H), 1.18 (*t*, *J*=6.5 Hz, 3H). $[MH]^+$ m/z=433.1.

*Procedure for alkylation of 8-((phenylamino)methyl)-2,3-dihydro-[1,4]dioxino[2,3-g]quinolin-7(6H)-one (**15**).*

Sodium hydride, 60% dispersion in mineral oil (200 mg, 5 mmol) was washed on a glass filter with anhydrous THF, then added to a solution of 8-((phenylamino)-methyl)-2,3-dihydro-[1,4]dioxino[2,3-g]quinolin-7(6*H*)-one (**15**) (308 mg, 1 mmol) in anhydrous DMF (10 mL) and the mixture was stirred at rt for 30 min. Then the reaction mixture was heated to 40 ºC, and the 2-chloro-*N*-(2-fluorophenyl)acetamide (**5e**) (225 mg, 1.2 mmol) was slowly added. The resulting mixture was stirred for 4 h at 70 °C, cooled to rt and diluted with water (40 mL). The formed precipitate was filtered off, washed with water, and recrystallized from i-PrOH to get a pure product **(16)** with an 88% yield.

*N-(2-fluorophenyl)-2-(7-oxo-8-((phenylamino)methyl)-2,3-dihydro-[1,4]dio-xino[2,3-g]quinolin-6(7H)-yl)acetamide (**16**).*

White powder, mp>300 °C. ^{1}H NMR: (200 MHz, DMSO-d6) δ 10.25 (*s*, 1H), 7.89 (*m*, 1H), 7.62 (*s*, 1H), 7.37–6.95 (*m*, 6H), 6.88 (*s*, 1H), 6.65–6.42 (*m*, 3H), 6.10 (*t*, *J*=6 Hz, 1H), 5.17 (*s*, 2H), 4.40–4.00 (*m*, 6H). $[MH]^+$ m/z=460.2.

5. Discussion of research results

SARS-CoV-2 inhibitors can be broadly categorized based on the enzymes they target [1, 3, 32, 33]. One major type is the M^{pro} non-covalent inhibitors, represented clinically by Ensitrelvir [8, 34, 35]. These inhibitors bind to the M^{pro} enzyme without forming covalent bonds; instead, they engage through hydrogen bonds, ionic interactions, and hydrophobic interactions to inhibit its activity [36]. Another type includes non-covalent inhibitors that hinder the function of the PL^{pro} enzyme [37, 38]. Consequently, both M^{pro} and PL^{pro} inhibitors have become pivotal in the efforts to inhibit SARS-CoV-2 activity [1, 39].

To identify dual-acting inhibitors, we began by selecting from our local evolutionary library using 3D pharmacophores derived from the available X-ray structure of the ligand-protease complex (PDB 7EN8). The molecular mechanisms of binding for M^{pro} and PL^{pro} were analyzed using the PLIP (Protein-Ligand Interaction Profiler) application and the Pharmit resource, which allows for interactive exploration of chemical space. This process enabled us to identify common binding parameters suitable for both M^{pro} and PL^{pro} [40].

The initial Evolutionary library consisted of 70k ligands and was filtered by M^{pro} pharmacophore screening (PDB: 7EN8), leading to Data hit-molecules 1 composed of 378 ligands. The further PL^{pro} pharmacophore screening (PDB: 8UUG) of this database led to Data hit-molecules 2 composed of 42 ligands (Fig. 4). Docking for the resulting Data hit-molecules 2 allowed to identify ligands whose binding Affinity value (kcal/mol) was at least 90 % or exceeded the corresponding value for the reference ligand of the ligand-protease complex M^{pro} and PL^{pro}. Further molecular docking of these ligands into the active sites of the M^{pro} and PL^{pro} proteases and calculating their binding energies allowed us to discover 5 ligands and their corresponding scaffolds capable of dual inhibition potential.

Our strategy for selecting dual-acting inhibitors targeting M^{pro} and PL^{pro} has several advantages over conventional virtual screening of single-acting small-molecule agents [33]. As a result, our selected hits show promise for greater inhibitory potency and broader spectrum activity against SARS-CoV-2 and its variants. This *novel approach* aligns with recent reports highlighting the effectiveness of targeting multiple SARS-CoV-2 proteins using direct molecular docking calculations [41].

In addition to notable advances in selecting and filtering dual-target SARS-CoV-2 inhibitors, our study provides *practical applications* for the theoretical results obtained [36]. For the selected hits, we developed and implemented efficient retrosynthetic procedures. The synthetic route for 2-(6-ethyl-4-oxoquinolin-1(4H)-yl)-N-(phenyl)-acetamide derivatives (6a-d), as shown in Fig. 12, proceeded through key intermediates (4a-c) via the Gold-Jacobs reaction of dimethylaminomethylene-benzoyl acetate (1) with 4-ethylaniline (2).

Practical relevance. The long-term goal in the fight against COVID-19 is to discover new pharmaceutical agents that can simultaneously inhibit the M^{pro} and PL^{pro} proteases of the SARS-CoV-2 virus. Our proposed in silico screening protocol aims to guide and streamline the drug development process. The practical significance of our study lies in identifying five potential hit ligands, which were then subjected to retrosynthetic analysis and subsequently synthesized for further in vitro biological activity testing.

Study limitations. The antiviral activity of the synthesized derivatives has not been evaluated yet. Therefore, the potential therapeutic effect of the selected derivatives is only based on theoretical predictions.

Prospects for further research. The suggested computer-aided protocol for *in silico* screening dual-acting inhibitors against M^{pro} and PL^{pro} of coronavirus SARS-CoV-2 has a strong potential for developing novel, promising antiviral agents.

6. Conclusions

A SARS-CoV-2 coronavirus life cycle depends on its cysteine proteases, making them promising targets for developing antiviral drugs to combat COVID-19. Among available antiviral strategies, developing new drugs that can target multiple viral proteins at once is of an emergent priority. Here, we analyze the molecular mechanisms of how non-covalent inhibitors interact with the main protease (M^{pro}) and papain-like (PL^{pro}) protease of SARS-CoV-2 to create a computer modelling algorithm for ligands that can inhibit both M^{pro} and PL^{pro} simultaneously.

In our study, we analyzed available X-ray data of SARS-CoV-2 protease-ligand binding complexes containing the potent non-covalent inhibitors. This analysis allowed us to identify some important structural features of the M^{pro} and PL^{pro} ligands. By matching and comparing the pharmacophore models of both M^{pro} and PL^{pro} ligands, we were able to identify a set of ligands that could potentially match the binding sites of both proteases. An evolutionary library was created by the DataWarrior program using the structures of the identified dual-acting ligands. Virtual screening and filtering of this library using both M^{pro} and PL^{pro} pharmacophores revealed several new hit ligands. Finally, after identifying these 5 potential hit-ligands, we developed retrosynthetic methods and obtained them for further *in vitro* biological activity studies. These findings can be further studied *in vitro* with the aim of discovering drugs for COVID-19.

Conflict of interest

The authors declare that they have no conflict of interest in relation to this research, whether financial, personal, authorship or otherwise, that could affect the research, and its results presented in this article.

Funding

The grant No. 87/0062 (2021.01/0062) “Molecular design, synthesis and screening of new potential antiviral pharmaceutical ingredients for the treatment of infectious diseases COVID-19” from the National Research Foundation of Ukraine.

Data availability

The manuscript has no associated data.

Use of artificial intelligence

The authors confirm that they did not use artificial intelligence technologies when creating the current work**.**

Acknowledgements

We thank Prof. T. Langer for giving us the opportunity to utilize the LigandScout 4.5 suite.

References

1. Yevsieieva, L. V., Lohachova, K. O., Kyrychenko, A., Kovalenko, S. M., Ivanov, V. V., Kalugin, O. N. (2023). Main and papain-like proteases as prospective targets for pharmacological treatment of coronavirus SARS-CoV-2. RSC Advances, 13 (50), 35500–35524. https://doi.org/10.1039/d3ra06479d

2. Abel, R., Paredes Ramos, M., Chen, Q., Pérez-Sánchez, H., Coluzzi, F., Rocco, M. et al. (2020). Computational Prediction of Potential Inhibitors of the Main Protease of SARS-CoV-2. Frontiers in Chemistry, 8. https://doi.org/10.3389/fchem.2020.590263

3. Zagórska, A., Czopek, A., Fryc, M., Jończyk, J. (2024). Inhibitors of SARS-CoV-2 Main Protease (Mpro) as Anti-Coronavirus Agents. Biomolecules, 14 (7), 797. https://doi.org/10.3390/biom14070797

4. Han, H., Gracia, A. V., Røise, J. J., Boike, L., Leon, K., Schulze-Gahmen, U. et al. (2023). A covalent inhibitor targeting the papain-like protease from SARS-CoV-2 inhibits viral replication. RSC Advances, 13 (16), 10636–10641. https://doi.org/10.1039/d3ra00426k

5. Prajapati, J., Patel, R., Rao, P., Saraf, M., Rawal, R., Goswami, D. (2022). Perceiving SARS-CoV-2 Mpro and PLpro dual inhibitors from pool of recognized antiviral compounds of endophytic microbes: an in silico simulation study. Structural Chemistry, 33 (5), 1619–1643. https://doi.org/10.1007/s11224-022-01932-0

6. Diogo, M. A., Cabral, A. G. T., de Oliveira, R. B. (2024). Advances in the Search for SARS-CoV-2 Mpro and PLpro Inhibitors. Pathogens, 13 (10), 825. https://doi.org/10.3390/pathogens13100825

7. Shi, Y., Dong, L., Ju, Z., Li, Q., Cui, Y., Liu, Y. et al. (2023). Exploring potential SARS-CoV-2 Mpro non-covalent inhibitors through docking, pharmacophore profile matching, molecular dynamic simulation, and MM-GBSA. Journal of Molecular Modeling, 29 (5). https://doi.org/10.1007/s00894-023-05534-3

8. Unoh, Y., Uehara, S., Nakahara, K., Nobori, H., Yamatsu, Y., Yamamoto, S. et al. (2022). Discovery of S-217622, a Noncovalent Oral SARS-CoV-2 3CL Protease Inhibitor Clinical Candidate for Treating COVID-19. Journal of Medicinal Chemistry, 65 (9), 6499–6512. https://doi.org/10.1021/acs.jmedchem.2c00117

9. Shionogi Announces Xocova® (Ensitrelvir Fumaric Acid) Obtained Standard Approval in Japan for the Treatment of SARS-CoV-2 Infection (2024). Shionogi. Available at: https://www.shionogi.com/global/en/news/2024/03/20240305.html

10. Qomara, W. F., Primanissa, D. N., Amalia, S. H., Purwadi, F. V., Zakiyah, N. (2021). Effectiveness of Remdesivir, Lopinavir/Ritonavir, and Favipiravir for COVID-19 Treatment: A Systematic Review. International Journal of General Medicine, 14, 8557–8571. https://doi.org/10.2147/ijgm.s332458

11. Huynh, T., Cornell, W., Luan, B. (2021). In silico Exploration of Inhibitors for SARS-CoV-2’s Papain-Like Protease. Frontiers in Chemistry, 8. https://doi.org/10.3389/fchem.2020.624163

12. Sivakumar, D., Stein, M. (2021). Binding of SARS-CoV Covalent Non-Covalent Inhibitors to the SARS-CoV-2 Papain-Like Protease and Ovarian Tumor Domain Deubiquitinases. Biomolecules, 11 (6), 802. https://doi.org/10.3390/biom11060802

13. Di Sarno, V., Lauro, G., Musella, S., Ciaglia, T., Vestuto, V., Sala, M. et al. (2021). Identification of a dual acting SARS-CoV-2 proteases inhibitor through in silico design and step-by-step biological characterization. European Journal of Medicinal Chemistry, 226, 113863. https://doi.org/10.1016/j.ejmech.2021.113863

14. Tumskiy, R. S., Tumskaia, A. V., Klochkova, I. N., Richardson, R. J. (2023). SARS-CoV-2 proteases Mpro and PLpro: Design of inhibitors with predicted high potency and low mammalian toxicity using artificial neural networks, ligand-protein docking, molecular dynamics simulations, and ADMET calculations. Computers in Biology and Medicine, 153, 106449. https://doi.org/10.1016/j.compbiomed.2022.106449

15. Kattula, B., Reddi, B., Jangam, A., Naik, L., Adimoolam, B. M., Vavilapalli, S. et al. (2023). Development of 2-chloroquinoline based heterocyclic frameworks as dual inhibitors of SARS-CoV-2 MPro and PLPro. International Journal of Biological Macromolecules, 242, 124772. https://doi.org/10.1016/j.ijbiomac.2023.124772

16. Kyrychenko, A., Bylov, I., Geleverya, A., Kovalenko, S., Zhuravel, I., Fetyukhin, V., Langer, T. (2024). Computer-aided rational design and synthesis of new potential antihypertensive agents among 1,2,3-triazole-containing nifedipine analogs. ScienceRise: Pharmaceutical Science, 3 (49), 4–12. https://doi.org/10.15587/2519-4852.2024.291626

17. Lohachova, K. O., Sviatenko, A. S., Kyrychenko, A., Ivanov, V. V., Langer, T., Kovalenko, S. M., Kalugin, O. N. (2024). Computer-aided drug design of novel nirmatrelvir analogs inhibiting main protease of Coronavirus SARS-CoV-2. Journal of Applied Pharmaceutical Science, 14 (5), 232–239. https://doi.org/10.7324/japs.2024.158114

18. Shen, J.-X., Du, W.-W., Xia, Y.-L., Zhang, Z.-B., Yu, Z.-F., Fu, Y.-X., Liu, S.-Q. (2023). Identification of and Mechanistic Insights into SARS-CoV-2 Main Protease Non-Covalent Inhibitors: An In-Silico Study. International Journal of Molecular Sciences, 24 (4), 4237. https://doi.org/10.3390/ijms24044237

19. Wolber, G., Langer, T. (2004). LigandScout: 3-D Pharmacophores Derived from Protein-Bound Ligands and Their Use as Virtual Screening Filters. Journal of Chemical Information and Modeling, 45 (1), 160–169. https://doi.org/10.1021/ci049885e

20. Lipinski, C. A., Lombardo, F., Dominy, B. W., Feeney, P. J. (2012). Experimental and computational approaches to estimate solubility and permeability in drug discovery and development settings. Advanced Drug Delivery Reviews, 64, 4–17. https://doi.org/10.1016/j.addr.2012.09.019

21. Sander, T., Freyss, J., von Korff, M., Rufener, C. (2015). DataWarrior: An Open-Source Program For Chemistry Aware Data Visualization And Analysis. Journal of Chemical Information and Modeling, 55 (2), 460–473. https://doi.org/10.1021/ci500588j

22. RCSB Protein Data Bank. Available at: https://www.rcsb.org

23. Goodsell, D. S., Morris, G. M., Olson, A. J. (1996). Automated docking of flexible ligands: Applications of AutoDock. Journal of Molecular Recognition, 9(1), 1–5. https://doi.org/10.1002/(sici)1099-1352(199601)9:1<1::aid-jmr241>3.0.co;2-6

24. Trott, O., Olson, A. J. (2009). AutoDock Vina: Improving the speed and accuracy of docking with a new scoring function, efficient optimization, and multithreading. Journal of Computational Chemistry, 31 (2), 455–461. https://doi.org/10.1002/jcc.21334

25. Protein-Ligand Interaction Profiler. Available at: https://plip-tool.biotec.tu-dresden.de/plip-web/plip/index

26. Pharmit. Available at: https://pharmit.csb.pitt.edu

27. Adasme, M. F., Linnemann, K. L., Bolz, S. N., Kaiser, F., Salentin, S., Haupt, V. J., Schroeder, M. (2021). PLIP 2021: expanding the scope of the protein–ligand interaction profiler to DNA and RNA. Nucleic Acids Research, 49 (W1), W530–W534. https://doi.org/10.1093/nar/gkab294

28. Sunseri, J., Koes, D. R. (2016). Pharmit: interactive exploration of chemical space. Nucleic Acids Research, 44 (W1), W442–W448. https://doi.org/10.1093/nar/gkw287

29. Anokhin, D., Kovalenko, S., Trostianko, P., Kyrychenko, A., Zakharov, A., Zubatiuk, T. et al. (2024). Towards the discovery of molecules with anti-COVID-19 activity: Relationships between screening and docking results. Kharkiv University Bulletin. Chemical Series, 42, 6–14. https://doi.org/10.26565/2220-637X-2024-42-01

30. Silin, O. V., Savchenko, T. I., Kovalenko, S. M., Nikitchenko, V. M., Ivachtchenko, A. V. (2004). Synthesis of Novel 5H-Pyrazolo[4,3-c]quinolines. Heterocycles, 63 (8), 1883–1890. https://doi.org/10.3987/com-04-10092

31. Savchenko, T. I., Silin, O. V., Kovalenko, S. M., Musatov, V. I., Nikitchenko, V. M., Ivachtchenko, A. V. (2007). Alkylation of 3-Phenyl-1H-pyrazolo[4,3-c] quinoline: Theoretical Analysis of Regioselectivity. Synthetic Communications, 37 (8), 1321–1330. https://doi.org/10.1080/00397910701227077

32. Xiao, Y.-Q., Long, J., Zhang, S.-S., Zhu, Y.-Y., Gu, S.-X. (2024). Non-peptidic inhibitors targeting SARS-CoV-2 main protease: A review. Bioorganic Chemistry, 147, 107380. https://doi.org/10.1016/j.bioorg.2024.107380

33. Yang, Y., Luo, Y.-D., Zhang, C.-B., Xiang, Y., Bai, X.-Y., Zhang, D., Fu, Z.-Y. et al. (2024). Progress in Research on Inhibitors Targeting SARS-CoV-2 Main Protease (Mpro). ACS Omega, 9 (32), 34196–34219. https://doi.org/10.1021/acsomega.4c03023

34. Tyndall, J. D. A. (2022). S-217622, a 3CL Protease Inhibitor and Clinical Candidate for SARS-CoV-2. Journal of Medicinal Chemistry, 65 (9), 6496–6498. https://doi.org/10.1021/acs.jmedchem.2c00624

35. Kawajiri, T., Kijima, A., Iimuro, A., Ohashi, E., Yamakawa, K., Agura, K. et al. (2023). Development of a Manufacturing Process toward the Convergent Synthesis of the COVID-19 Antiviral Ensitrelvir. ACS Central Science, 9 (4), 836–843. https://doi.org/10.1021/acscentsci.2c01203

36. Song, L., Gao, S., Ye, B., Yang, M., Cheng, Y., Kang, D. et al. (2024). Medicinal chemistry strategies towards the development of non-covalent SARS-CoV-2 Mpro inhibitors. Acta Pharmaceutica Sinica B, 14 (1), 87–109. https://doi.org/10.1016/j.apsb.2023.08.004

37. Taylor, A. J., Amporndanai, K., Rietz, T. A., Zhao, B., Thiruvaipati, A., Wei, Q. et al. (2024). Fragment-Based Screen of SARS-CoV-2 Papain-like Protease (PLpro). ACS Medicinal Chemistry Letters, 15 (8), 1351–1357. https://doi.org/10.1021/acsmedchemlett.4c00238

38. Magwaza, N. N., Mushebenge, A. G.-A., Ugbaja, S. C., Mbatha, N. A., Khan, R. B., Kumalo, H. M. (2024). Mechanistic Insights into Targeting SARS-CoV-2 Papain-like Protease in the Evolution and Management of COVID-19. BioChem, 4 (3), 268–299. https://doi.org/10.3390/biochem4030014

39. Schimunek, J., Seidl, P., Elez, K., Hempel, T., Le, T., Noé, F. et al. (2023). A community effort in SARS-CoV-2 drug discovery. Molecular Informatics, 43 (1). https://doi.org/10.1002/minf.202300262

40. Ivanov, V., Lohachova, K., Kolesnik, Y., Zakharov, A., Yevsieieva, L., Kyrychenko, A. et al. (2023). Recent advances in computational drug discovery for therapy against coronavirus SARS-CoV-2. ScienceRise: Pharmaceutical Science, 6 (46), 4–24. https://doi.org/10.15587/2519-4852.2023.290318

41. Puhl, A. C., Godoy, A. S., Noske, G. D., Nakamura, A. M., Gawriljuk, V. O., Fernandes, R. S. et al. (2023). Discovery of PLpro and Mpro Inhibitors for SARS-CoV-2. ACS Omega, 8 (25), 22603–22612. https://doi.org/10.1021/acsomega.3c01110

Received 16.09.2024
Received in revised form 07.11.2024
Accepted 14.11.2024
Published 19.11.2024

Larysa Yevsieieva, Senior Lecturer, School of Chemistry, V. N. Karazin Kharkiv National University, Svobody sq., 4, Kharkiv, Ukraine, 61022

Pavlo Trostianko, PhD Student, School of Chemistry, V. N. Karazin Kharkiv National University, Svobody sq., 4, Kharkiv, Ukraine, 61022

Alexander Kyrychenko*, Doctor of Chemical Sciences, Senior Researcher, School of Chemistry, V. N. Karazin Kharkiv National University, Svobody sq., 4, Kharkiv, Ukraine, 61022

Volodymyr Ivanov, Doctor of Chemical Sciences, Professor, School of Chemistry, V. N. Karazin Kharkiv National University, Svobody sq., 4, Kharkiv, Ukraine, 61022

Sergiy Kovalenko, Doctor of Chemical Sciences, Professor, School of Chemistry, V. N. Karazin Kharkiv National University, Svobody sq., 4, Kharkiv, Ukraine, 61022

Oleg Kalugin, PhD, Professor, School of Chemistry, V. N. Karazin Kharkiv National University, Svobody sq., 4, Kharkiv, Ukraine, 61022

***Corresponding author:** *Alexander Kyrychenko, e-mail: a.v.kyrychenko@karazin.ua*